Chemical Physics 352 (2008) 97–105

Contents lists available at ScienceDirect

Chemical Physics

journal homepage: www.elsevier.com/locate/chemphys

Excited state absorption and decay kinetics of near IR polymethine dyes

Lazaro A. Padilha [a], Scott Webster [a,*], Honghua Hu [a], Olga V. Przhonska [a,c], David J. Hagan [a,b], Eric W. Van Stryland [a,b], Mikhail V. Bondar [c], Iryna G. Davydenko [d], Yuriy L. Slominsky [d], Alexei D. Kachkovski [d]

[a] CREOL & FPCE, The College of Optics and Photonics, University of Central Florida, Orlando, FL 32816, United States
[b] Department of Physics, University of Central Florida, Orlando, FL 32816, United States
[c] Institute of Physics, National Academy of Sciences, Prospect Nauki 46, Kiev 03028, Ukraine
[d] Institute of Organic Chemistry, National Academy of Sciences, Murmanskaya 5, Kiev 03094, Ukraine

ARTICLE INFO

Article history:
Received 13 February 2008
Accepted 16 May 2008
Available online 22 May 2008

Keywords:
Polymethine
Structure–property relations
Symmetry breaking
Cyanine
Terminal groups
Charge delocalization
Excited state absorption
Two photon absorption
Z-Scan
Pump probe
Nonlinear absorption

ABSTRACT

We performed a detailed experimental investigation and quantum-chemical analysis of linear, excited state absorption (ESA) spectra, and lifetime dynamics of a new series of near IR symmetrical cationic polymethine dyes, with 5-butyl-7,8-dihydrobenzo[*cd*]furo[2,3-*f*]indolium terminal groups. Additionally, two neutral dyes, squaraine and tetraone, were synthesized with the same terminal groups. We compare the nonlinear absorption properties of these three dyes with an analogous set of three "visible" dyes with simpler benzo[*e*]indolium terminal groups. Measurements are performed using laser systems with femtosecond and picosecond pulsewidths. We find that the dyes with dihydrobenzo[*cd*]furo[2,3-*f*]indolium terminal groups are characterized by a remarkably large red shift (200–300 nm) of their linear and excited state absorption bands. The absorption bands for these dyes can now be shifted systematically to the near IR region by a contribution from their terminal group that strongly increases the total length of conjugation. ESA spectra in the "near IR" set of molecules have strong absorption bands with excited state absorption cross sections increasing from 2×10^{-16} cm^2 for the shortest polymethine chain (trimethine cyanine) to 9×10^{-16} cm^2 for the longer chain (heptamethine cyanine). The peak ESA magnitude for heptamethine cyanine is approximately twice as large compared to its peak ground state absorption, but the oscillator strengths of the two bands are almost equal. This observation indicates that the ESA oscillator strengths can be as large as those of ground state transitions. The results of these experiments combined with agreement of the quantum-chemical calculations move us closer to a predictive capability for molecular structure–nonlinear properties relations of cyanine-like molecules.

1. Introduction

Strong and selective absorption across a broad spectral region of cyanine and cyanine-like dyes have made them attractive for applications as fluorescent probes in chemistry and biology, active and passive laser media, photosensitizers, optical data storage and electroluminescence materials [1–5]. The structural modification of dyes, allowing a shift of their absorption bands to the near infrared (NIR) region, can expand the existing areas of applications and reveal new ones such as highly efficient nonlinear optical materials for all-optical signal processing [6]. In spite of the increasing information available about near IR absorbing dyes, their thermal stabilities, photochemical stabilities, and solubilities are the main issues limiting their practical applications. Most of the known synthetic methods to decrease the energy gap between the ground and excited states consist of lengthening the polymethine chain usually leading to a decrease in photochemical stability. By novel chemical modifications to the terminal groups, we have bypassed this difficulty with the purpose of improving their functionality for the previously mentioned applications. The main absorption band for these dyes can now be shifted systematically to the near IR region by increasing the contribution from the terminal groups to the total length of conjugation. In this work we analyze the excited state absorption spectra (ESA) and lifetime dynamics of cyanine structures, introduced in our previous manuscript Ref. [16], with specific terminal groups of dihydrobenzo[*cd*]furo[2,3-*f*]indolium, which have their own extended π conjugation system, which in turn can interact strongly with the main chromophore. This leads to an increase of the total conjugation without increasing the length of the chromophore and without decreasing its photochemical stability.

In order to understand the origin of charge localization on some specific molecular orbitals, local orbitals that are connected with the structure of the terminal groups, and how those orbitals influence the linear and nonlinear absorption, we synthesized

* Corresponding author. Tel.: +1 407 823 6864.
E-mail address: swebster@creol.ucf.edu (S. Webster).

0301-0104/$ - see front matter © 2008 Elsevier B.V. All rights reserved.
doi:10.1016/j.chemphys.2008.05.007

and studied a new series of near IR symmetrical cationic polymethines with 5-butyl-7,8-dihydro-benzo[*cd*]furo[2,3-*f*]indolium terminal groups with different chain lengths (number of vinylene groups increases from $n = 1$–4). Compared to dyes with the same chain length but simpler terminal groups, such as indolium or benzo[*e*]indolium studied in previous articles [7,8], we notice a remarkably large shift of ~300 nm in their linear absorption bands to the near IR region.

We synthesized and studied two additional neutral dyes, squaraine and tetraone, with identical terminal groups and acceptor bridges in the main conjugation backbone in order to gain a better understanding of the relations between structure and nonlinear absorption properties. The nonlinear characterization has been based on detailed spectroscopic studies and focused on measuring ESA spectra over a broad spectral range and investigating their excited-state decay kinetics. We show that these dyes can satisfy two requirements important for nonlinear optical applications. First, the new dyes are characterized by sufficiently large ground state absorption cross sections to nearly completely populate the excited state (i.e., $\geqslant 10^{-18}$ cm^2) over a large portion of the visible spectrum. Secondly, their excited state absorption cross sections are of the order of 10^{-16}–10^{-15} cm^2 at the peak, which is comparable with the peak ground state absorption cross section values. This produces a large difference between excited and ground state cross sections with cross section ratios up to 100.

In this paper we will describe: (1) the electronic structure of near IR dyes along with their linear absorption and fluorescence properties (more details can be found in Ref. [16]), (2) the experimental methods used for nonlinear absorption measurements including femtosecond pump-white light continuum probe and *Z*-scans in the pico- and femtosecond time regimes, (3) a detailed analysis of the ESA spectra and their decay kinetics, (4) comparison of nonlinear properties of near IR dyes with their counterparts dyes in the visible region, and (5) quantum-chemical analyses allowing us to understand the nature of the linear absorption and ESA bands. The combination of these methods gives us information about the dye's energy level structure, which accurately predicts the nonlinear absorption properties in cyanine-like molecules.

2. Experimental methods and results

2.1. Materials and linear characterization

The molecular structures of the dyes studied in this paper are shown in Figs. 1 and 2. Their chemical names are: 5-butyl-4-[3-(5-butyl-8-methyl-7,8-dihydrobenzo[*cd*]furo[2,3-*f*]indol-4(5*H*)-ylidene)prop-1-enyl]-8-methyl-7,8-dihydrobenzo[*cd*]furo[2,3-*f*]indol-5-ium tetrafluoro-borate (labeled as PD 2371); 5-butyl-4-[5-(5-butyl-8-methyl-7,8-dihydro-benzo[*cd*]furo[2,3-*f*]indol-4(5*H*)-ylidene)penta-1,3-dienyl]-8-methyl-7,8-dihydrobenzo[*cd*]furo[2,3-*f*]indol-5-ium tetrafluoroborate (labeled as PD 2658), 5-butyl-4-[7-(5-butyl-8-methyl-7,8-dihydro-benzo[*cd*]furo[2,3-*f*]indol-4(5*H*)-ylidene)hepta-1,3,5-trienyl]-8-methyl-7,8-dihydrobenzo[*cd*]-furo-[2,3-*f*]indol-5-ium tetrafluoroborate (labeled as PD 2716), 5-butyl-4-(3-{3-[3-(5-butyl-8-methyl-7,8-dihydrobenzo[*cd*]furo[2,3-*f*]indol-4(5*H*)-ylidene)prop-1-enyl]-5,5-dimethylcyclo-hex-2-en-1-yli-d- ene}prop-1-enyl)-8-methyl-7,8-dihydrobenzo[*cd*]furo[2,3-*f*]indol-5-ium tetra-fluoroborate (labeled as PD 2892). These dyes differ by the length of polymethine chromophore (number of vinylene groups $n = 1$–4). Corresponding tetracarbocyanine PD 2892 includes a trimethylene bridge in the chromophore to increase

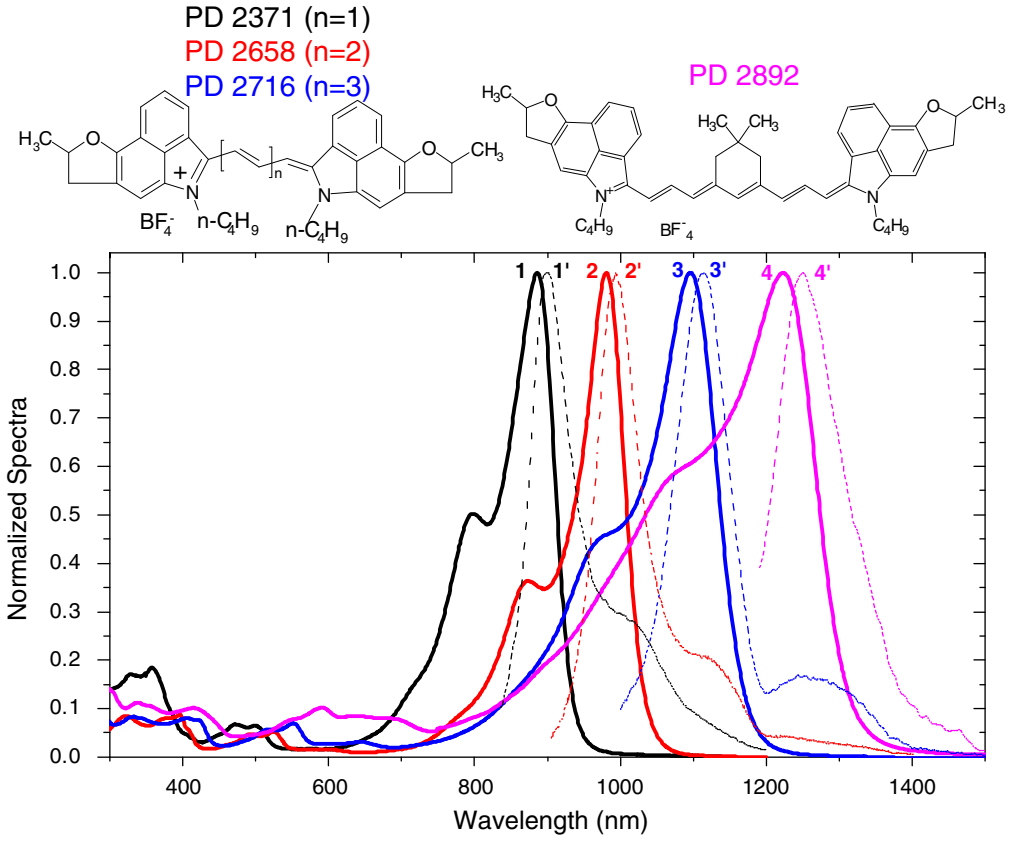

Fig. 1. Molecular structures, linear absorption, and fluorescence spectra for PD 2371 (1,1′), PD 2658 (2,2′), PD 2716 (3,3′), and PD 2892 (4,4′), respectively, in butanol. (For interpretation of the references to colour in this figure legend, the reader is referred to the web version of this article.)

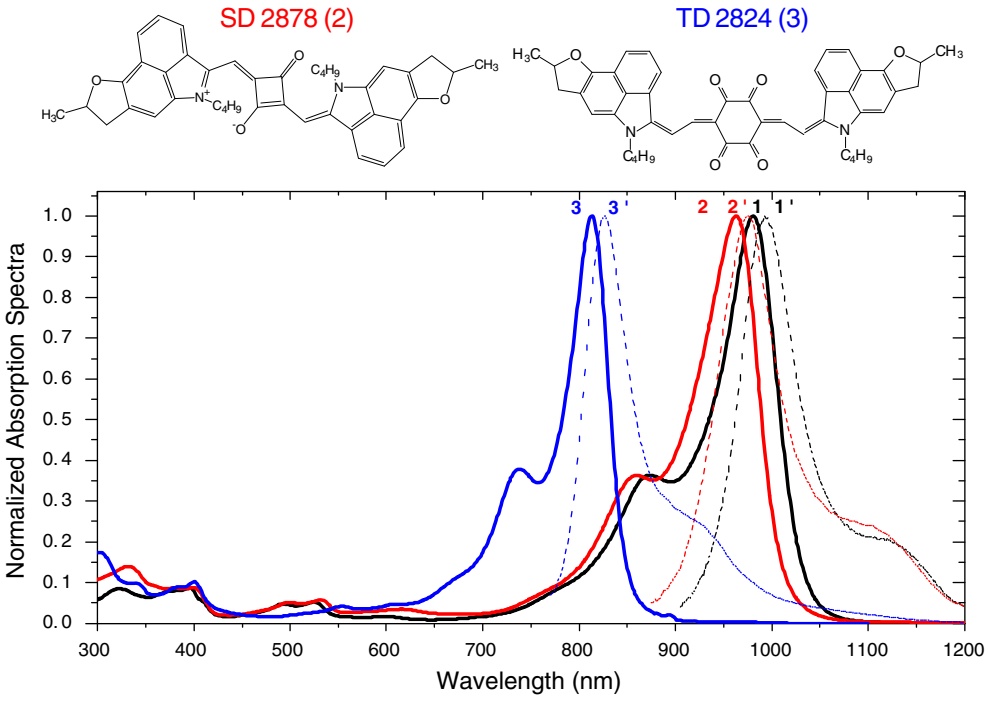

Fig. 2. Molecular structures, linear absorption, and fluorescence spectra for PD 2658 (1,1′), SD 2878 (2,2′), TD 2824 (3,3′). Note: structure for PD 2658 is shown in Fig. 1. (For interpretation of the references to colour in this figure legend, the reader is referred to the web version of this article.)

thermal- and photostability. Additionally, the salt labeled as 2337 was synthesized with an identical structure and compared with the terminal groups in the corresponding dyes. Based on the structure of dicarbocyanine PD 2658, two new compounds: squaraine 4-[(5-butyl-8-methyl-7,8-dihydrobenzo[*cd*]furo[2,3-*f*]indol-5-ium-4-yl)methylene]-2-[(5-butyl-8-methyl-7,8-dihydrobenzo[*cd*]furo[2,3-*f*]indol-4(5*H*)-ylidene)methyl]-3-oxocyclobut-1-en-1-olate (labeled as SD 2878) and tetraone 3,6-Bis[2-(5-butyl-8-methyl-7,8-dihydrobenzo[*cd*]furo[2,3-*f*]indol-4(5*H*)-ylidene)ethylidene]cyclohexane-1,2,4,5-tetrone (labeled as TD 2824) were synthesized and investigated. The last two molecules possess the same 5-butyl-7,8-dihydrobenzo[*cd*]furo[2,3-*f*]indolium terminal groups and similar conjugation lengths for the purpose of performing a comparative analysis of the influence of increasing the acceptor bridge strength on the optical properties. We also perform a comparison of the linear and nonlinear properties of this set of near IR dyes (PD 2658, SD 2878, and TD 2824) and a set of visible dyes (PD 2630, SD 2243, and TD 2765), which were investigated by us previously, with the only difference being in the terminal groups and their effect on the effective conjugation length [8,9]. The extinction coefficients for the investigated dyes in butanol are: $0.99 \times 10^5\ M^{-1}\ cm^{-1}$ at a peak position of 885 nm for PD 2371, $2.11 \times 10^5\ M^{-1}\ cm^{-1}$ at a peak position of 980 nm for PD 2658, $1.37 \times 10^5\ M^{-1}\ cm^{-1}$ at a peak position of 1096 nm for PD 2716, $1.18 \times 10^5\ M^{-1}\ cm^{-1}$ at a peak position of 1223 nm for PD 2892, $1.71 \times 10^5\ M^{-1}\ cm^{-1}$ at a peak position of 963 nm for SD 2878, and $1.76 \times 10^5\ M^{-1}\ cm^{-1}$ at a peak position of 813 nm for TD 2824.

The linear absorption and fluorescence spectra of all molecules, shown in Figs. 1 and 2, are recorded with a Varian Cary 500 spectrophotometer and PTI QuantaMaster spectrofluorimeter equipped with nitrogen cooled (77 K) Hamamatsu R5509-73 photomultiplier. All fluorescence spectra are corrected with the spectral responsivity of the photomultiplier tube and spectrofluorimeter. A substantial broadening of the absorption bands for the longest PDs represented by the growth of the short wavelength shoulder was previously explained theoretically with the concept of soliton-ic-like waves of charge density and alternating bond lengths [10–14] and experimentally [10,15] by a symmetry breaking effect. Based on the experimental studies of the absorption shapes in solvents of different polarities, we suggest that this symmetry breaking effect may be observed in this series of cyanines starting from $n = 3$. In contrast to absorption spectra, fluorescence spectra for all dyes are narrow independent of the solvent polarity indicating that emission originates from the symmetrical form only. More detailed information about the spectroscopic properties of these near IR dyes with dihydrobenzo[*cd*]furo[2,3-*f*]indolium terminal groups, including quantum yield measurements, may be found in Ref. [16].

The absorption and fluorescence spectra of PD 2658, SD 2878, and TD 2824 are shown in Fig. 2. All dyes have the same donor (D) terminal groups, but squaraine and tetraone molecules include an acceptor (A) bridge in the main conjugation backbone and therefore represent the structure: D–π–A–π–D. PD 2658 and SD 2878 have the same chain length ($n = 2$) with an odd number of carbon atoms, however the tetraone dye TD 2824 belongs to a polyene-like family of compounds with an even number of carbon atoms in the conjugated chain. Having the same terminal groups and similar length of conjugation, this dye contains a stronger acceptor bridge. The absorption bands of SD 2878 and TD 2824 (especially TD 2824 as a polyene structure) are blue shifted when compared to the corresponding PD 2658. These shifts correlate with increasing electron acceptor strength in the bridge leading to a decrease in effective conjugation length due to bond lengthening in the acceptor groups [9].

2.2. Nonlinear characterization

Nonlinear optical characterization of the near IR dyes has been focused on the ESA spectra and lifetime dynamics investigations. Measurements are performed using laser systems with femtosecond and picosecond pulsewidths. The femtosecond system is a Clark-MXR 2010 regeneratively amplified Ti:sapphire laser operat-

ing at 1 kHz at 775 nm with ~2 mJ per pulse, which pumps two optical parametric generator/amplifiers (OPG/OPA Light Conversion Ltd., model TOPAS), providing 100–140 fs pulsewidths (FWHM) with independently tunable wavelengths from 0.3 to 2.3 μm. The picosecond laser system consists of a 10 Hz mode-locked Nd:YAG laser (EKSPLA, model PL2143) with a measured pulsewidth of 21 ps (FWHM) at 1064 nm and externally frequency doubled to produce 532 nm with a measured pulsewidth of 15 ps (FWHM).

To measure the ESA spectra, a femtosecond pump – white light continuum probe technique is used as described in Ref. [17]. Briefly, the output from one of the independently tunable OPG/OPAs is set to the absorption peak for the pump. The second OPG/OPA is sent through a calcium fluoride plate to generate a sub-picosecond white light continuum probe. The probe delay time is set to ~1 ps to avoid pump-probe overlapping in time while remaining shorter than the excited state lifetime. The white light probe is then referenced and spatially overlapped with the pump in the sample and spectrally resolved upon transmission using a spectrometer (Acton Research Corp, model SpectraPro 2500i). The incident angle between pump and probe is ~5°. The ESA spectrum, $\sigma_{1i}(\lambda)$, is then calculated using Eq. (1):

$$T_L(\lambda) = \exp[-\sigma_{01}(\lambda)NL]$$
$$T_{NL}(\lambda) = \exp[-\sigma_{01}(\lambda)N_0L - \sigma_{1i}(\lambda)N_1L] \quad (1)$$

where $T_L(\lambda)$ is the linear transmittance measured by a linear spectrophotometer and $T_{NL}(\lambda)$ is the nonlinear transmittance of the probe beam in the presence of the pump. The variables $\sigma_{01}(\lambda)$ and $\sigma_{1i}(\lambda)$ are ground and excited state absorption cross sections and N is the total number of molecules per unit volume, which equals the sum of concentrations of the molecules in the ground (N_0) and the first excited state (N_1) in the approximation that we can neglect the populations of any other levels, and L is the sample length. To determine absolute values of $\sigma_{1i}(\lambda)$, we use $\sigma_{1i}(\lambda_{ESA})$ data obtained from independent pico- and femtosecond Z-scan measurements at different wavelengths, typically close to ESA peaks for each molecule (λ_{ESA}), using Eq. (2) from Ref. [15] as reproduced here

$$\sigma_{1i}(\lambda) = \sigma_{01}(\lambda) - (\sigma_{01}(\lambda_{ESA}) - \sigma_{1i}(\lambda_{ESA})) \times (\ln[T_{NL}/T_L]|_\lambda)/(\ln[T_{NL}/T_L]|_{\lambda_{ESA}}). \quad (2)$$

Experimentally measured ESA spectra for all molecules studied and their decay kinetics are shown in Figs. 3 and 4 and discussed in Section 3.2.

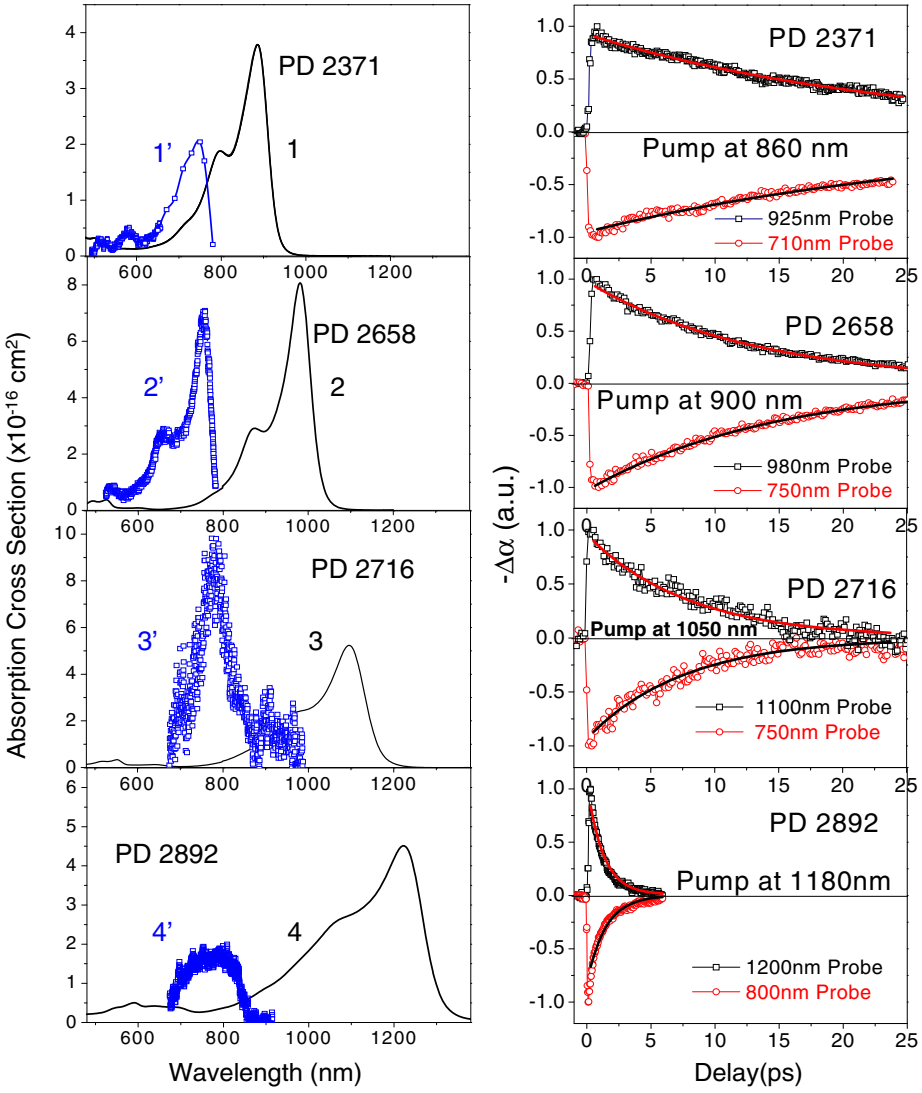

Fig. 3. Linear and excited state absorption spectra for PD 2371 (1,1″), PD 2658 (2,2′), PD 2716 (3,3′) and PD 2892 (4,4′) in butanol. Their decay kinetics are shown to the right (Δα is a change of the absorption of the probe beams).

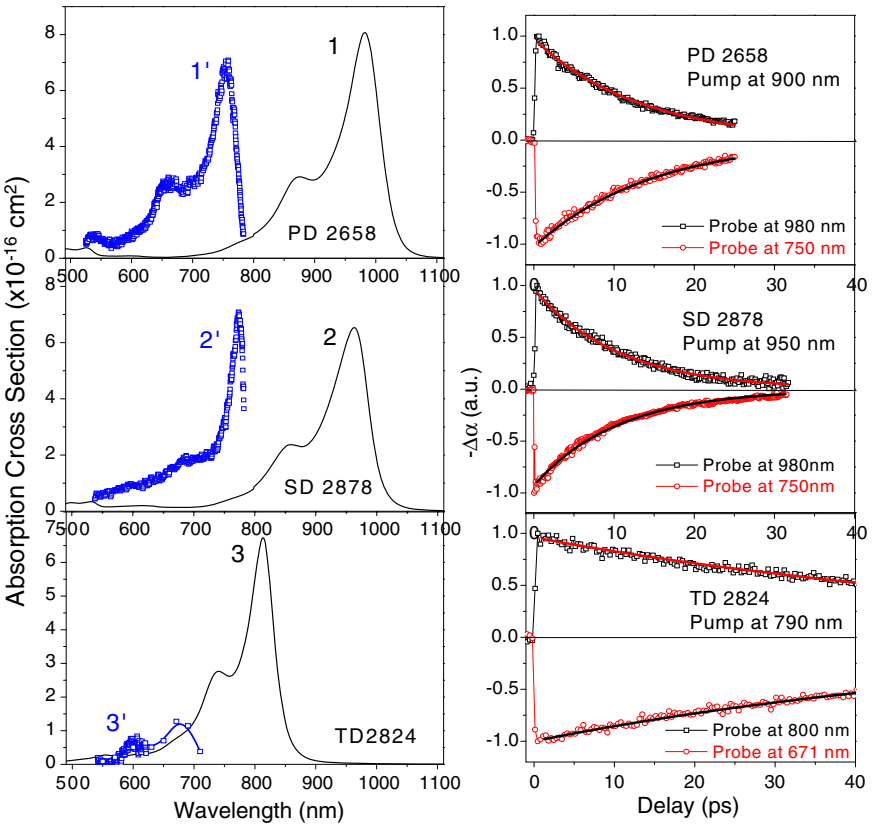

Fig. 4. Linear and excited state absorption for PD 2658 (1,1′), SD 2878 (2,2′), TD 2824 (3,3′). Their decay kinetics are shown to the right ($\Delta\alpha$ is a change of the absorption of the probe beams).

In order to understand and model nonlinear absorption properties, the fluorescence lifetimes and population dynamics must be understood. Estimation of lifetimes performed from the steady state fluorescence measurements indicate that all dyes are characterized by very short lifetimes, which requires the use of femtosecond pulsewidths. The femtosecond nondegenerate measurements of the decay kinetics for each dye were performed using a pump wavelength near the linear absorption peak and at two probe wavelengths: (1) within the ESA band at a spectral region of reverse saturable absorption, RSA, and (2) at a wavelength closer to the linear absorption peak at a spectral region of saturable absorption, SA. The results are shown in Figs. 3 and 4. The decay kinetics for each dye follows a monoexponential decay with similar lifetimes for both cases, RSA and SA, confirming that the excited-state depopulation and restoration of the ground state population display the same lifetimes. Therefore, there are no additional intermediate states having a significant lifetime. More detailed decay dynamics for several probe wavelengths are presented for PD 2658 in Fig. 5a. The wavelength of the pump beam is chosen to be within the main absorption band at 900 nm; the decay dynamics at different probe wavelengths show an evolution of nonlinear kinetics from an RSA region (probing at 800 nm, 750 nm and 650 nm) to a SA region (probing at 980 nm and 830 nm). As shown, all curves for PD 2658 show the same monoexponential decay with a lifetime of $\tau_F = 12 \pm 2$ ps. The largest amplitude of RSA and SA correspond to the ESA peak at 750 nm and the linear absorption peak at 980 nm. The range between 800 nm and 830 nm corresponds to the crossing area where RSA is changing to SA and ground and excited-state cross sections become equal.

Fig. 5b represents an interesting case for a comparison between a white light continuum probe and a single wavelength probe for PD 2658. In both cases, the pump wavelength is fixed at 900 nm. First, we probe the ESA region at 780 nm; curve 4 corresponds to a single wavelength probe and curve 3 corresponds to a white light continuum probe. Experimentally, this relates to a position of the spike filter (which transmits the probe at 780 nm from the white light continuum) placed before the sample (curve 1) and after the sample (curve 2). Second, we probe the SA region in the same way; curve 1 corresponds to a single wavelength probe (spike filter transmitting the probe at 1000 nm placed before the sample) and curve 2 corresponds to a white light continuum probe (spike filter placed after the sample). Fig. 5b demonstrates the striking difference between the decay kinetics presented by curves 1 and 2 and by 3 and 4, respectively. As observed, the decay kinetics in the case of a white light continuum probe consists of two components. The fast component being of ≈300 fs (resolution of our femtosecond system is 150–200 fs) reflects the changes in the ground or excited state populations due to stimulated emission processes. Fig. 1 demonstrates the large overlapping area between the absorption and fluorescence bands (small Stokes shift). This implies that a white light continuum probe stimulates a fast depopulation of the excited state. From this comparison, we note the significance of stimulating excited state depopulation with multiple probe wavelengths in the region of absorption and fluorescence overlap. Therefore, a spike filter is used before the sample to avoid stimulated depopulation and to accurately measure the excited state lifetimes.

Measurements show that lifetimes for the molecules in butanol are as follows: $\tau_F = 30 \pm 5$ ps for PD 2371, $\tau_F = 12 \pm 2$ ps for PD 2658, $\tau_F = 7 \pm 2$ ps for PD 2716, $\tau_F = 1.3 \pm 0.5$ ps for PD 2892, $\tau_F = 11 \pm 2$ ps for SD 2878, and $\tau_F = 75 \pm 10$ ps for TD 2824. Triplet states are not expected in this class of molecules, as confirmed experimentally from the recovery of the transmittance. Therefore, triplet states can be neglected for nonlinear absorption modeling. Molec-

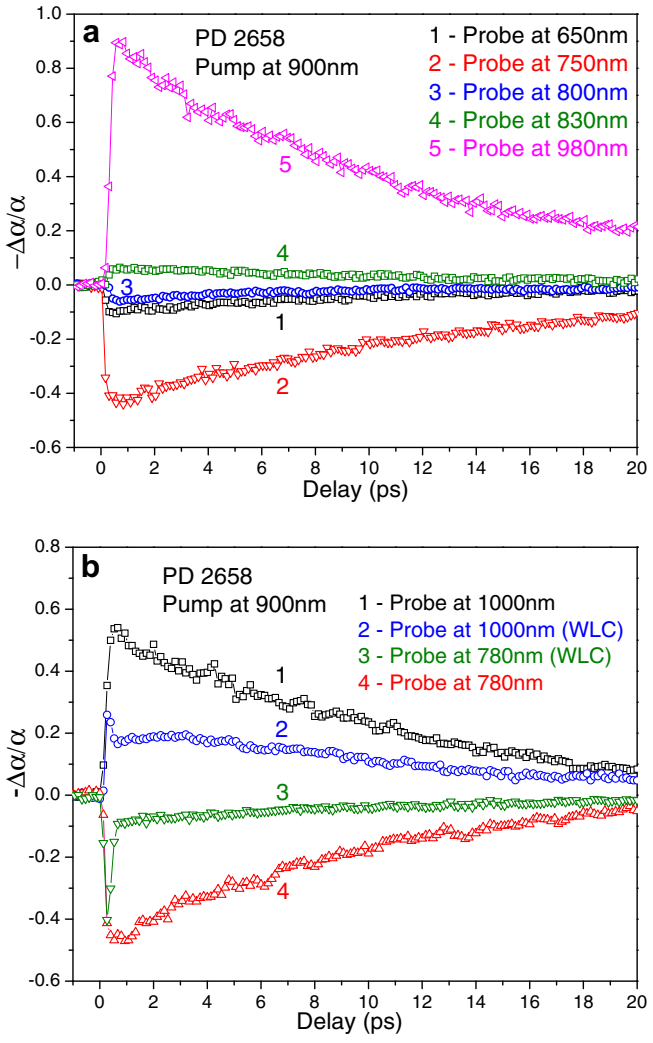

Fig. 5. (a) Decay dynamics for the several probe beams for PD 2658 at pump 900 nm. (b) Comparison between white light continuum (WLC) probe and a single wavelength probe for PD 2658 at pump 900 nm. ($\Delta\alpha$ is a change of the absorption of the probe beams).

ular reorientation times, which are known to depend on solvent polarity and molecular volumes, are much longer than fluorescence lifetimes (on the order of 10^2 picoseconds), and therefore cannot affect the lifetime measurements for these dyes [18–20].

The absolute values of ESA cross sections are obtained with open aperture *Z*-scan [21] measurements by applying the modeling of Ref. [9]. These measurements are performed in the picosecond regime for all the dyes except PD 2892, which has the shortest lifetime of ~1.3 ps, for which we use femtosecond *Z*-scans. A comparison of picosecond and femtosecond *Z*-scan measurements was performed for PD 2716 and resulted in similar ESA cross sections. All measurements are made at several fluences and different wavelengths close to the ESA peak for each molecule: 580 nm for PD 2371, 740 nm for PD 2658, 760 nm for PD 2716, 740 nm for PD 2892 (shown in Fig. 3), 770 nm for SD 2878, and 600 nm for TD 2824 (shown in Fig. 4). Focused spot sizes are calibrated at each wavelength by measuring closed aperture *Z*-scan of a neat solution of carbon disulfide CS_2 as a Ref. [22]. To extract ESA cross sections, *Z*-scan results are modeled by RSA and fit with a three-level model taking into account singlet levels only. Propagation and rate equations are described by Eqs. (3):

$$\begin{aligned}
\frac{dI}{dz} &= -\sigma_{01}N_0 I - \sigma_{12}N_1 I \\
\frac{dN_0}{dt} &= -\frac{\sigma_{01}N_0 I}{\hbar\omega} + \frac{N_1}{\tau_F} \\
\frac{dN_1}{dt} &= \frac{\sigma_{01}N_0 I}{\hbar\omega} - \frac{N_1}{\tau_F} - \frac{\sigma_{12}N_1 I}{\hbar\omega} + \frac{N_2}{\tau_{21}} \\
\frac{dN_2}{dt} &= -\frac{\sigma_{12}N_1 I}{\hbar\omega} - \frac{N_2}{\tau_{21}}
\end{aligned} \tag{3}$$

where $N = N_0 + N_1 + N_2$, τ_F is determined from femtosecond pump-probe measurements, and τ_{21} is the decay lifetime of the S_2 level. Experimental data for *Z*-scans and their fitting with this three-level model for several molecules are shown in Fig. 6 and discussed in Section 3.2.

3. Discussion of results and quantum-chemical approach

3.1. Quantum-chemical approach

Quantum-chemical orbital analysis is performed with the goal of understanding the formation of the linear absorption spectra [16] and ESA bands in the series of near IR dyes with 5-butyl-

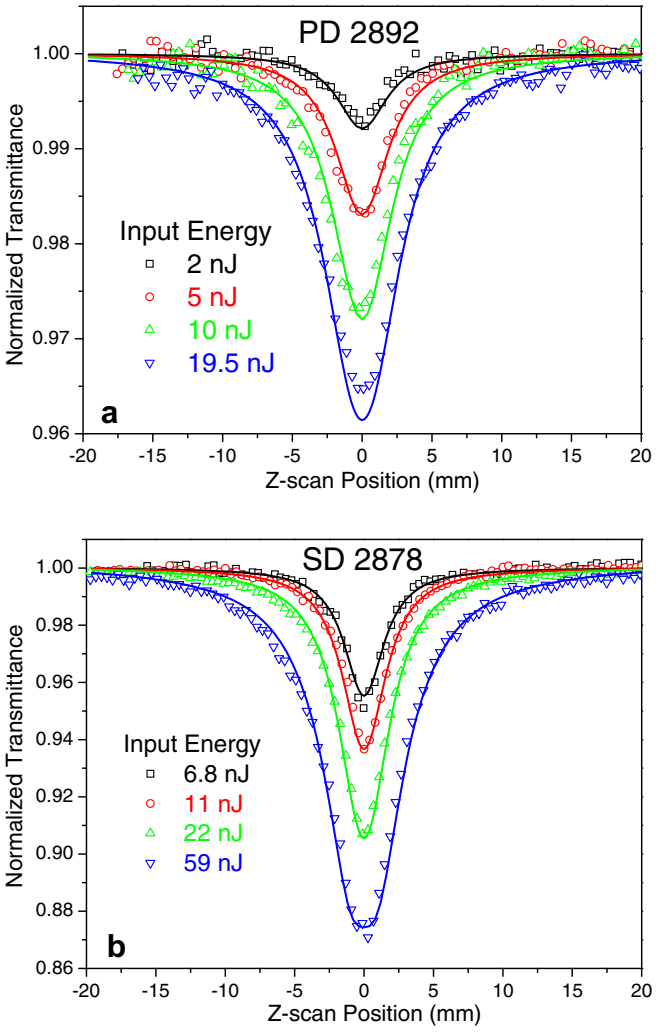

Fig. 6. Open aperture *Z*-scan measurements using (a) 140 fs (FWHM) at 740 nm for PD 2892; (b) 14 ps (FWHM) at 770 nm for SD 2878. Solid lines are fits using the 3-level model with the following parameters (a) $\sigma_{01} = 2.64 \times 10^{-17}$ cm^2, $\sigma_{12} = 1.5 \times 10^{-16}$ cm^2, $\tau_{10} = 1.5$ ps, and $\tau_{21} = 500$ fs (b) $\sigma_{01} = 5.05 \times 10^{-17}$ cm^2, $\sigma_{12} = 6.6 \times 10^{-16}$ cm^2, $\tau_{10} = 13$ ps, and $\tau_{21} = 3$ ps.

7,8-dihydrobenzo[*cd*]furo[2,3-*f*]indolium terminal groups. The methodology for the calculations of the positions of the electronic levels and the shapes of their molecular orbitals is described in Refs. [7,8]. This orbital approach is a very useful tool for understanding the nature of the orbitals and of the transitions between them. It has been applied previously for getting a complete picture of the nonlinear absorption properties, including two-photon and excited state absorption of the visible PD-SD-TD dyes [9]. The optimized molecular geometries for all investigated molecules were calculated in the HyperChem package, AM1 approximation [23]. The energies of the molecular orbitals (MOs), electronic transitions between them and oscillator strengths were calculated in the framework of the standard semi empirical ZINDO/S method [24]. The wavefunctions of the excited states were built with the configuration interaction technique taking into account 7 occupied and 3 unoccupied MOs, a total of 21 configurations. In our calculations, we limited the number of molecular orbitals considered to allow explanation of the experimentally observed ESA bands in the visible and near IR region.

Fig. 7 represents the schemes of the highest occupied MO (HOMO), several occupied MOs below HOMO, lowest unoccupied molecular orbital (LUMO), the next LUMO + 1, the shapes of MOs, and transition paths for PD 2658. The wave function of the *i*th MO φ_i was written as an expansion of the atomic orbitals $\chi_\mu : \varphi_i = \sum_\mu C_{i\mu}\chi_\mu$, where the $C_{i\mu}$ are the corresponding coefficients, and the summation runs over all atomic orbitals. We note that $C^2_{i\mu}$ is the probability of the location of an electron in the *i*th MO in the neighborhood of the μth atom [8]. The shapes of MOs presented in Fig. 7 correspond to coefficients $C_{i\mu}$ allowing to analyze the symmetry of the wave function φ_i.

Quantum-chemical orbital analysis allows a distinction between three types of molecular orbitals (MO): (1) two donor occupied orbitals HOMO and HOMO-1, originating from the donor nitrogen atoms and extending to the chain, (2) local occupied orbitals originating primarily from the benzene rings of the terminal groups (HOMO-2, HOMO-3 in Fig. 7), and (3) delocalized occupied HOMO-4 and unoccupied LUMO spreading out over the chain. Note that symmetrical and asymmetrical pairs of donor and local orbitals are formed from the doubly degenerate orbitals as a result of their splitting, leading to charge redistribution. Therefore, transitions between these orbitals are characterized by very different oscillator strengths. A more detailed description of the nature of the different types of orbitals can be found in our previous article [9]. The first allowed $S_0 \rightarrow S_1$ transition for all molecules is connected with electron transfer from HOMO to LUMO. It is important to take into account that the position of the LUMO for all cationic PDs is almost independent of the molecular topology; charge is distributed mainly over the chain. Therefore, this energy level may be presented as a "charge" or "solitonic level". As a result, we may conclude that the $S_0 \rightarrow S_1$ transition energy for PDs depends mainly on the position of the donor HOMO level. Note that this level may be significantly shifted for neutral molecules, such as SDs and TDs. An increase in the chain length (corresponding to an increase in the number of π-electrons) leads to a higher energy position of the HOMO and a decrease of the energy gap between HOMO and LUMO levels. As was previously mentioned, PDs with dihydrobenzo[*cd*]furo[2,3-*f*]indolium terminal groups absorb at much longer wavelengths (up to 300 nm longer) as compared to dyes with the same conjugation length but the simpler terminal groups, such as indolium or benzo[*e*]indolium. The large red shift is connected with a more extended conjugated system including the terminal groups moving their HOMO to higher energy positions.

The next $S_0 \rightarrow S_2$ transition for all dyes primarily involves the asymmetrical donor HOMO-1 and asymmetrical LUMO. This transition of the $1A_1 \rightarrow 2A_1$ symmetry is characterized by a much smaller oscillator strength and corresponds to the experimentally observed small absorption bands at ≈570 nm for PD 2371, ≈615 nm in PD 2658, and ≈648 nm in PD 2716 in the less polar solvent *o*-dichlorobenzene (which more accurately corresponds

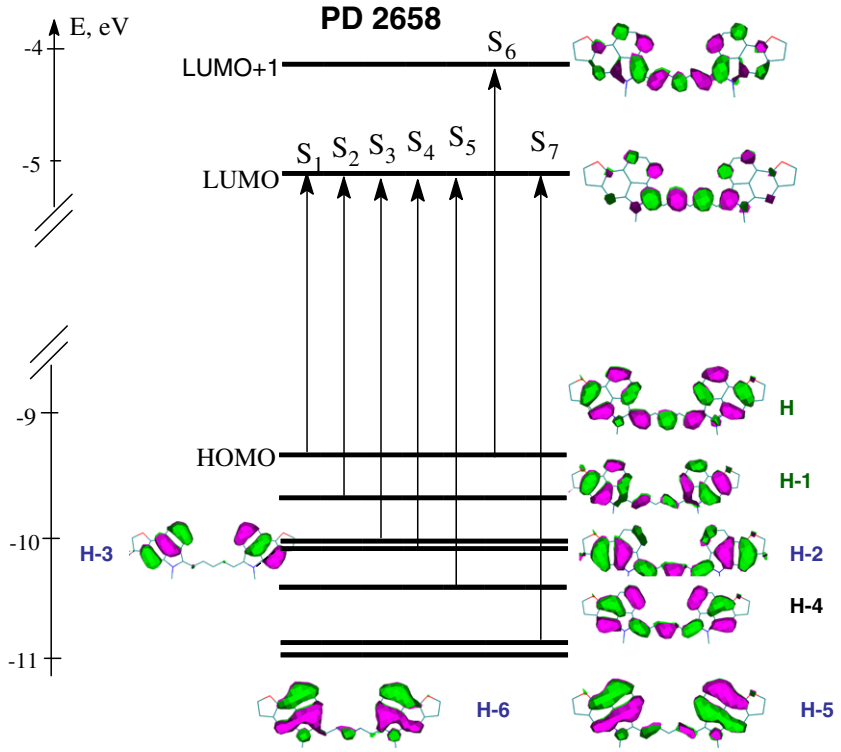

Fig. 7. Schematic of molecular orbital (MO) energy levels with corresponding transitions and charge density distribution for PD 2658.

to data from quantum-chemical calculations). In tetracarbocyanine, PD 2892, this band is covered by the shoulder of the $S_0 \rightarrow S_1$ band. It is important to note that quantum-chemical calculations indicate a large energy splitting between the two donor molecular orbitals HOMO and HOMO-1. This results in a large separation (~300 nm) between the $S_0 \rightarrow S_1$ and $S_0 \rightarrow S_2$ transitions. In contrast, the corresponding separation for the visible dyes (with indolium or benzo[*e*]indolium terminal groups) is less than 150 nm. Two next transitions, $S_0 \rightarrow S_3$ and $S_0 \rightarrow S_4$, for all of the dyes corresponds to the electron transfer from the symmetrical HOMO-2 and asymmetrical HOMO-3 local orbitals to the LUMO. These bands originate from the molecular orbitals localized at the terminal groups and correspond to the lowest absorption band of the salt 2337. They show a systematic red shift of ≈30 nm with an increase of chain length from PD 2371 to PD 2892 without a significant change in spectral shape. The next transition, $S_0 \rightarrow S_5$, involves charge transfer from HOMO-4, which is delocalized over the whole molecule, to the same LUMO level. The nature of the next two transitions, $S_0 \rightarrow S_6$ and $S_0 \rightarrow S_7$, for all the molecules is more complicated and involves transitions from HOMO-5 to LUMO and from HOMO to the higher LUMO + 1 level. Calculations show that the terminal groups are much more involved in all transitions as compared to the dyes with simpler terminal groups (indolium and benzo[*e*]indolium), as can be seen from a comparison of the visible and UV absorption spectra of the near IR dyes and the corresponding salt.

3.2. Excited state absorption

Quantum-chemical calculations and molecular orbital analyses allow estimation of the positions of the ESA bands, the dipole orientation relative to that of the main band, $S_0 \rightarrow S_1$, as well as the MOs responsible for the ESA magnitude. The ESA transitions can be roughly calculated as the energy difference between the transitions of the $1A_1 \rightarrow nA_1$ symmetry and the main linear absorption peak assuming that there are no substantial changes in the excited-state molecular geometry upon excitation. For cyanine-like molecules, the intramolecular relaxation upon excitation is small as evidenced by the small Stokes shifts and near mirror symmetry of the absorption and fluorescence spectra.

The experimentally measured ESA bands for all near IR molecules are shown in Figs. 3 and 4. First, we examine the positions of the ESA spectra as a function of conjugation length compared with that of the linear absorption spectra. The linear absorption peaks shift by ~300 nm, while the ESA peaks shift by only 60–70 nm. The same trend was observed by us earlier for the series of PDs with the simpler terminal groups and different chain length from $n = 2$ to $n = 5$, however, the total shift of their ESA spectra was found to be twice as large [20]. Based on this comparison, we may conclude that the terminal groups in this series of near IR dyes play a major role in the formation of the ESA spectra. This is confirmed by quantum-chemical analysis provided below and the experimental comparison between the ESA peak positions for near infrared dye PD 2658 and visible dye PD 2630 shown in Ref. [9]. Both dyes have the same conjugation length, and a 200 nm red shift in ESA position for PD 2658 is convincing evidence of the effect of the dihydrobenzo[*cd*]furo[2,3-*f*]indolium terminal groups.

Next, we examine the peak values of ESA cross sections, σ_{ex}, in comparison with the peak ground state absorption cross sections, σ_{01}. As seen from Figs. 3 and 4, all ESA spectra represent strong bands with σ_{ex} increasing from 2×10^{-16} cm^2 for the shortest PD 2371 to 9×10^{-16} cm^2 for PD 2716. The last value is approximately twice as large as the peak ground state absorption cross section. It is also instructive to compare the integrated area of the absorption bands since these are proportional to the oscillator strength of the transition. The main characteristic to note is that as the conjugation length is increased, the areas of the linear and ESA absorption bands become closer to one another in magnitude. The integrated area of the ESA absorption band for PD 2716 is nearly 95% of the ground state leading to the conclusion that excited state oscillator strength can be as large as that of the ground state transition. This is in accord with our previous findings that an increase in the length of the polymethine chromophore leads to an increase of the excited state cross sections [20]. We now conclude that a similar increase can be achieved by changing the nature of the terminal groups. The ESA cross section for the longest molecule PD 2892 is smaller, $\sigma_{ex} \approx 2 \times 10^{-16}$ cm^2, which may be connected with ESA from unrelaxed vibrational sublevels of S_1 due to the use of femtosecond pulses for this measurement.

We performed a detailed comparison between the ESA spectra for the near IR squaraine and tetraone dyes with the visible ones described in Ref. [9]. The experimental data are shown in Fig. 4. ESA spectra for both near IR dyes show a substantial red shift of ≈200 nm (the same trend as for PDs) for SD 2878 and ≈170 nm for TD 2824 clearly indicating the strong effect of the dihydrobenzo[*cd*]furo[2,3-*f*]indolium terminal groups. For SD 2878, the maximum $\sigma_{ex} \approx 7 \times 10^{-16}$ cm^2, which is about three times larger than that of the visible squaraine with the same conjugation length and the simpler benzo[*e*]indolium terminal groups [9]. However, for TD 2824, the maximum $\sigma_{ex} \approx 1.2 \times 10^{-16}$ cm^2 is about two times smaller than that of the visible tetraone. This is the only dye from the new series of near IR molecules, which for an unknown reason shows a relatively small excited state cross section value. For practical applications, the ratio σ_{ex}/σ_{01}, while keeping sufficiently large ground state cross sections (i.e., $\geqslant 10^{-18}$ cm^2), is an important parameter. The maximum σ_{ex}/σ_{01} for the visible PD 2630 is ≈20 at 515 nm, where as for near IR dyes PD 2658 and PD 2716 this ratio reaches ≈80 for 650 nm and ≈100 for 750 nm, respectively. For the visible and near IR squaraines, these ratios are comparable: maximum $\sigma_{ex}/\sigma_{01} \approx 15$–20 due to an increased ground state absorption for SD 2878. For the visible and near IR tetraones, these ratios are smaller: $\sigma_{ex}/\sigma_{01} \approx 5$.

According to our calculations, for all near IR cyanines there are several allowed ESA bands ($1B_1 \rightarrow nA_1$ symmetry) of different intensities in the spectral range of 400 to 1500 nm. Two weak ESA bands, corresponding mainly to mixing between HOMO-1 and HOMO-3 with HOMO, are placed near ~1500 nm and ~1000 nm. The most intense ESA bands observed experimentally are placed in the range of ~750–780 nm and correspond to LUMO → LUMO + 1 transitions analogous to the ESA bands in the series of visible PD-SD-TD dyes, as was shown by us previously [9]. However, ESA bands in the previously studied dyes were connected with LUMO and LUMO + 1 orbitals, which are delocalized mainly within the polymethine chain as in the unsubstituted molecules. For near IR dyes, LUMO and especially LUMO + 1 (see Fig. 7) involve charge distribution that extends into the terminal groups. This leads to a significant red shift of the ESA bands for these dyes up to ~200 nm. The nature of the less intense visible ESA bands (for example, 650 nm for PD 2658 and SD 2878 in Figs. 3 and 4) is more complicated for analysis and involves overlapping between several molecular orbitals.

4. Conclusions

We have described a detailed experimental investigation of the linear and nonlinear absorption properties of a new series of near IR cationic polymethine dyes and performed quantum-chemical analysis in order to understand the effect of dihydrobenzo[*cd*]furo[2,3-*f*]indolium terminal groups that extend the conjugation to these molecular extremities. We also synthesized and

studied two neutral dyes, squaraine and tetraone, with the same terminal groups to provide a deeper insight into structure–property relations and get a better understanding of the properties of cyanine-like molecules. We performed a comparison of the ESA spectra of this new set of "near IR" dyes (PD 2658, SD 2878, and TD 2824) with a set of "visible" dyes (PD 2630, SD 2243, TD 2765) with the simpler benzo[*e*]indolium terminal groups studied by us earlier [9]. From these measurements, we find that the dyes with dihydrobenzo[*cd*]furo[2,3-*f*]indolium terminal groups are characterized by a remarkably large shift of their linear and excited state absorption bands to the red region (200–300 nm). The large red shifts for the linear absorption bands in the "near IR" set of molecules (300 nm for PDs and 200 nm for SD) can be explained by the extended π-system within the terminal groups and their strong connection with the π-system of the chain resulting in a significant extension of the effective conjugation length as seen in our previous work [16]. The effect of these terminal groups is equivalent to the extension of the chain to three vinylene groups specifically for PDs with benzo[*e*]indolium terminal groups. Experimental data and quantum-chemical analysis allowed us to make the following conclusions:

1. The large red shifts for the ESA bands in the "near IR" set of molecules (∼200 nm) can also be explained by the strong effect of the terminal groups, but in a slightly different manner than the explanation of the linear shift. Quantum-chemical calculations show that the most intense ESA band corresponds to the LUMO → LUMO + 1 transition analogous to the ESA bands in the series of visible PD, SD, and TD dyes [9]. However, ESA bands in the previously studied "visible" set of dyes were connected with LUMO and LUMO + 1 orbitals, which are mainly delocalized within the polymethine chain as in the unsubstituted molecules. In contrast, LUMO and especially LUMO + 1 in the "near IR" set of molecules involve charge distributions that extend into the terminal groups.
2. ESA spectra in the "near IR" set of molecules represent strong bands with σ_{ex} increasing from 2×10^{-16} cm^2 for the shortest PD 2371 to 9×10^{-16} cm^2 for PD 2716. The last value is about two times larger than the peak ground state absorption cross section value for this dye. We performed a comparison of the integrated area of the ESA and linear absorption bands since they are directly related to the oscillator strength of the transitions and concluded that the lengthening of the conjugation length results in comparable strengths of the ground and excited state transitions. Thus, the integrated area of the ESA absorption band for PD 2716 is nearly 95% of that for the ground state area leading to the very important result that excited state oscillator strength can be as large as that of the ground state transition.
3. All near IR dyes are characterized by very short fluorescence lifetimes from ≈1.3 ps for PD 2892 to ≈75 ps for TD 2824 indicating a very fast channel of deactivation of the excited state energy. Our measurements for each dye show monoexponential decay kinetics with almost identical lifetimes for both reverse and saturable absorption cases. This confirms that excited-state depopulation and the restoration of the ground state population for each molecule exhibit the same lifetime.

Acknowledgments

We gratefully acknowledge the support of the National Science Foundation ECS 0524533, the US Army Research Laboratory W911NF0420012, the US Army Research Laboratory and the US Army Research Office under Contract/Grant Number 50372-CH-MUR, and the Office of Naval Research MORPH N00014-06-1-0897.

References

[1] A. Mishra, Chem. Rev. 100 (2000) 1973.
[2] F. Meyers, S.R. Marder, J.W. Perry, Chem. Adv. Mater. (1998) 207.
[3] H. Suzuki, K. Ogura, N. Matsumoto, P. Prosposito, S. Schutzmann, Mol. Cryst. Liq. Cryst. 444 (2006) 51.
[4] J. Fabian, Chem. Rev. 92 (1992) 1197.
[5] A.I. Tolmachev, Yu.L. Slominsky, A.A. Ishchenko, in: S. Daehne, U. Resh-Genge, U. Wolfbeis (Eds.), Dyes for High Technology Applications, Kluwer Academic Publishers., New York, 1998, p. 384.
[6] J.M. Hales, S. Zheng, S. Barlow, S.R. Marder, J.W. Perry, JACS 128 (2006) 11362.
[7] J. Fu, L.A. Padilha, D.J. Hagan, E.W. Van Stryland, O.V. Przhonska, M.V. Bondar, Yu.L. Slominsky, A.D. Kachkovski, JOSA B 24 (2007) 56.
[8] J. Fu, L.A. Padilha, D.J. Hagan, E.W. Van Stryland, O.V. Przhonska, M.V. Bondar, Yu.L. Slominsky, A.D. Kachkovski, JOSA B 24 (2007) 67.
[9] S. Webster, J. Fu, L.A. Padilha, O.V. Przhonska, D.J. Hagan, E.W. Van Stryland, M.V. Bondar, Yu.L. Slominsky, A.D. Kachkovski, Chem. Phys. 348 (2008) 143.
[10] L.M. Tolbert, X. Zhao, J. Am. Chem. Soc. 119 (1997) 3253.
[11] J.S. Craw, J.R. Reimers, G.B. Bacskay, A.T. Wong, N.S. Hush, Chem. Phys. 167 (1992) 77.
[12] J.S. Craw, J.R. Reimers, G.B. Bacskay, A.T. Wong, N.S. Hush, Chem. Phys. 167 (1992) 101.
[13] A.B. Ryabitsky, A.D. Kachkovski, O.V. Przhonska, THEOCHEM 802 (2007) 75.
[14] J. Fabian, THEOCHEM 766 (2006) 49.
[15] R.S. Lepkowicz, O.V. Przhonska, J.M. Hales, J. Fu, D.J. Hagan, E.W. Van Stryland, M.V. Bondar, Yu.L. Slominsky, A.D. Kachkovski, Chem. Phys. 305 (2004) 259.
[16] S. Webster, L.A. Padilha, H. Hu, O.V. Przhonska, D.J. Hagan, E.W. Van Stryland, M.V. Bondar, I. Davidenko, Yu.L. Slominsky, A.D. Kachkovski, J. Lumin., doi:10.1016/j.jlumin.2008.06.002.
[17] R.A. Negres, O.V. Przhonska, D.J. Hagan, E.W. Van Stryland, M.V. Bondar, Yu.L. Slominsky, A.D. Kachkovski, IEEE J. Quant. Elect. 7 (2001) 849.
[18] R.S. Lepkowicz, O.V. Przhonska, J.M. Hales, D.J. Hagan, E.W. Van Stryland, M.V. Bondar, Yu.L. Slominsky, A.D. Kachkovski, Chem. Phys. 286 (2003) 277.
[19] J.R. Lakowicz, Principles of Fluorescence Spectroscopy, second ed., Kluwer Academic/Plenum Publishers, New York, 1999.
[20] R.S. Lepkowicz, C.M. Cirloganu, J. Fu, O.V. Przhonska, D.J. Hagan, E.W. Van Stryland, M.V. Bondar, Y.L. Slominsky, A.D. Kachkovski, JOSA B 22 (2005) 2664.
[21] M. Sheik-Bahae, A.A. Said, T.-H. Wei, D.R. Hagan, E.W. Van Stryland, IEEE J. Quant. Elect. 26 (1990) 760.
[22] M. Sheik-Bahae, A.A. Said, E.W. Van Stryland, Opt. Lett. 14 (1989) 955.
[23] M.J.S. Dewar, E.G. Zoebisch, E.F. Healy, J.J.P. Stewart, J. Am. Chem. Soc. 107 (1985) 3902.
[24] M.C. Zerner, G.H. Loew, R.F. Kirchner, U.T. Mueller-Westerhoff, Am. Chem. Soc. 102 (1980) 589.